Information Sciences Letters
An International Journal

http://dx.doi.org/10.18576/isl/120111

Electrical and Magnetic Properties of Mn-Bi-Sb Alloys

A. M. Ahmed[*], *H. F. Mohamed, A. K. Diab and E. Y. Omar*

Physics Department, Faculty of Science, Sohag University, 82524 Sohag, Egypt

Received: 22 May 2022, Revised: 2 Jun. 2022, Accepted: 3 Aug. 2022.
Published online: 1 Jan. 2023

Abstract: $MnBi_{1-x}Sb_x$ alloys were prepared by the conventional melt technique. The Seebeck coefficient (S), electrical resistivity (ρ), and magnetic susceptibility (χ) were measured at various temperatures ranging from ~100 to 400 K. The electrical resistivity of $x \leq 0.15$ shows both semiconducting and metallic behavior depending on temperature and Sb content, whereas samples $x \geq 0.2$ have only semiconductor behavior in all the temperature range. The negative sign of the Seebeck coefficient increases, i.e., the positivity decreases with the increasing Sb content. The magnetic susceptibility (χ) shows that alloys undergo ferro-paramagnetic transition at a certain temperature (T_C) and the T_C values decrease with increasing Sb content. From thermoelectric measurements and electronic thermal conductivity calculated, it was observed that Sb doping increases the power factor (PF) and the figure of merit (ZT). Thus, Sb content plays an essential role in making these alloys applicable in the thermoelectric industry.

Keywords: Crystal structure, Magnetic properties, Figure of merit, Ternary alloy system, Thermoelectric power.

1. Introduction

The increasing demand of rare earth elements (REEs), for use in the manufacture of efficient permanent magnets, is an important factor in the cost and availability of the elements in the future. A comprehensive inventory of potential compounds for designing ground-free ferromagnetic materials has been carried out by Kramer et al. [1], where they discovered that the Earth-free ferromagnetic material is BiMn. Many researches showed the crystallization of BiMn in the hexagonal form (space group P63/mmc), and this structure is stable up to 353 °C [2]. Despite many intensive researches, it was not possible to synthesize BiMn as a bulk material without impurities (refs [3-7]).

To solve these problems, a third element such as Ni, Pt, or Rh is added to MnBi, which forms an intermetallic phase with Bi that is symmetrical with α-BiMn [8, 9]. In addition, some research has been done to partially substitute Bi by Sb, which forms two magnetic phases with Mn, i.e., Mn_2Sb and MnSb. Between these, hexagonal MnSb is isotopes with BiMn; where Bi and Sb are completely miscible with each other [10].

The electrical resistivity and thermo-electric power of the Mn-Bi-Sb alloy have not been published previously. Regarding the binary alloy Mn-Sb, Grazhdankina et al. [11] interpreted the sign change of the temperature coefficient of electrical resistivity in the region $T > T_C$ under the influence of pressure in the context of the Stoner -Wohlfarth band theory of ferromagnetism [12].

A series of $MnBi_{1-x}Sb_x$ alloys, $(0 \leq x \leq 0.15)$ were prepared by Truong Xuan Nguyen et al. [13]. The results appeared the fact that the Sb can substitute Bi entering the unit cell, which accelerated the diffusion process between ($Bi_{1-x}Sb_x$) and Mn to form MnBi low-temperature pressure (LTP).

The aim of this work is to successfully prepare ternary $MnBi_{1-x}Sb_x$ alloys. Thermoelectric power, electrical resistivity, and magnetic properties are studied as a function of both Sb concentration and ambient temperature for the first time.

2. Experimental:

The preparation method used for $MnBi_{1-x}Sb_x$ alloys is the same method described by Yamaguchi, Watanabe, and Suzuki [14]. The original chemically pure elements Mn (99.9%), Bi (99.99%), and Sb (99.9%) were mixed well and ground after taking the required proportions, then pressed into disk form and packed into a vacuum quartz ampoule. The synthesis of the alloys proceeded in two stages: (1) the pressed disks were placed in a furnace, where they remained for 24 h at 813 K, after which the furnace turned- off and left to cool to room temperature. (2) the alloys, blended by milling after the first stage of preparation, for 30 min to homogeneity and pressed into disk under the pressure of 3ton.cm^{-2}. The disk was placed in an evacuated quartz ampule, and annealed for 24 hours at 1273 K; then they were

[*]Corresponding author e-mail: a.ahmed@science.sohag.edu.eg

quenched in ice. The structural characterization was achieved by X-ray diffraction (XRD), which was carried out by a Brucker diffractometer (Axs-D8 Advance) at room temperature with CuK_α radiation (λ= 1.5406Å). The microstructures of the alloys were considered by scanning electron microscope (SEM). The electrical resistivity (ρ) and the Seebeck coefficient (S), were measured at various temperatures ranging from 100 to 300 K. A surface-to-surface contact method was used to measure ρ (T) in a variable temperature liquid nitrogen cryostat. The Seebeck coefficient measurement was carried out using the two-heater method with copper electrodes [15]. The temperature difference between the two opposing surfaces of the sample was set to 5K during the entire measurement. The AC susceptibility χ of the alloys was measured at 100–400K temperature range under a magnetic field of 250μT and the frequency of 0.3kHz using the Barrington Instruments MS2/MS3 susceptibility system [15].

3. Results and discussion

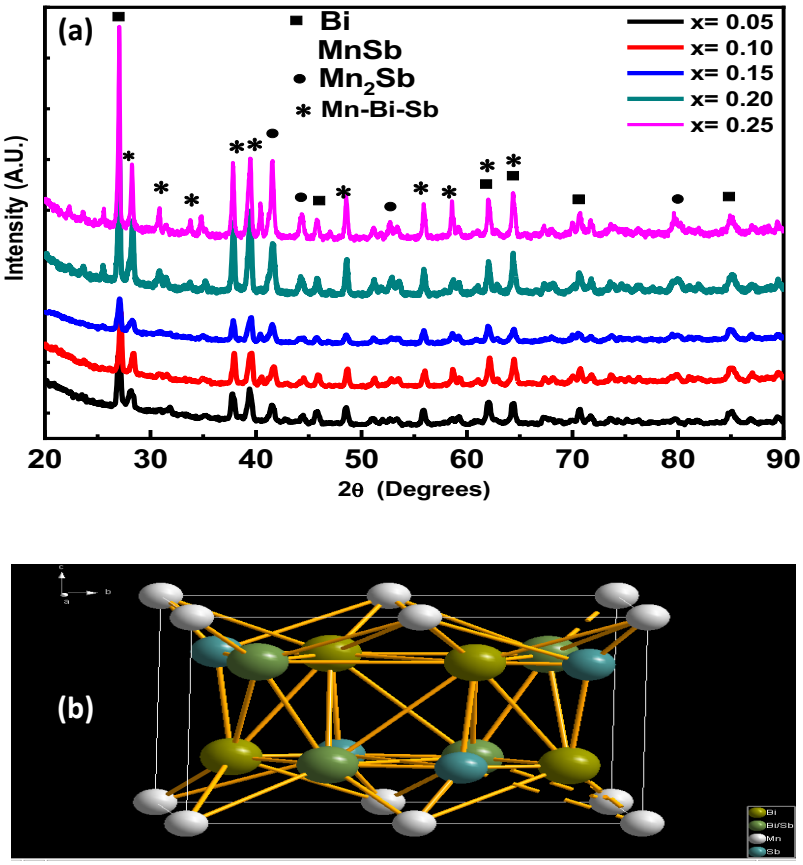

Fig. 1. (a) Powder XRD patterns for $MnBi_{1-x}Sb_x$ ($0.05 \leq x \leq 0.25$) alloys, (b) the schematic crystallographic structure of $MnBi_{1-x}Sb_x$alloys by Diamond software, color coding: olive Bi, petrol Sb, white Mn, dark olive Bi/Sb.

Figure. 1 shows the XRD patterns of the $MnBi_{1-x}Sb_x$ with x = 0.05, 0.10, 0.15, 0.20, & 0.25 at. %. In good agreement with earlier studies [13,16], we found that all the peaks belong to Bi, Mn_2Sb, MnSb and Mn-Bi-Sb phases. The emergence of separate bismuth has been observed at 2θ ~ 27.16, 45.76, 70.73 & 84.92°. The peaks of Mn_2Sb appeared at 2θ ~ 41.60, 44.33, 52.60 & 79.6°. The binary MnSb phase appeared at 2θ~ 40.46 & 71.70°. The ternary phase Mn-Bi-Sb is observed at 2θ ~ 28.3, 37.85, 39.4 & 48.6°. In addition, the appearance of Mn_2Sb, MnSb and MnBiSb phases point to the completion of the reaction between the elements Mn, Bi, and Sb. Thus, we can describe the crystal structure of the ternary phase with the composition Mn-Bi-Sb as hexagonal P63/mmc group, which was later confirmed by Gabay et al. [16], the second phase Mn_2Sb associated with the tetragonal P4/n mm (129) [17] and the bismuth phase allied hexagonal R-3m (166) [15-18]. As we can see from Figure (1-b) the schematic crystallographic structure of $MnBi_{1-x}Sb_x$ alloys designed by "Diamond" software.

By Sb doping, Mn and Sb are crystallized as MnSb and Mn_2Sb binary phases during the quenching and annealing process [10].

Table 1: Crystal structure parameters of $MnBi_{1-x}Sb_x$ ($0.05 \leq x \leq 0.25$) alloys

Crystal structure				
Empirical formula	$MnBi_{1-x}Sb_x$			
Space group	Hexagonal P63/mmc group			
Lattice parameters				
Sample (x)	**a(Å)**	**c(Å)**		**Cell volume (Å^3)**
0.05	8.692	5.772		656.756
0.10	8.689	5.697		656.176
0.15	8.687	5.695		655.626
0.20	8.687	5.697		655.479
0.25	8.683	5.732		654.538
Empirical formula	Mn_2Sb			
Space group	Tetragonal P4/n mm			
Lattice parameters				
Sample (x)	**a(Å)**	**c(Å)**	**c/a**	**Cell volume (Å^3)**
0.05	4.659	5.885	1.263	101.178
0.10	4.659	5.869	1.259	101.178
0.15	4.643	5.885	1.268	100.088
0.20	4.637	5.884	1.269	99.700
0.25	4.634	5.889	1.271	99.481
Empirical formula	Bi			
Space group	Hexagonal R-3m			
Lattice parameters				
Sample (x)	**a(Å)**	**c(Å)**	**c/a**	**Cell volume (Å^3)**
0.05	4.540	11.885	2.618	93.612
0.10	4.537	11.876	2.617	93.438
0.15	4.536	11.953	2.635	93.352
0.20	4.532	12.020	2.652	93.116
0.25	4.532	12.017	2.651	93.098
Crystallite size				
Samples (X)	**Average crystallite size ‹D_{WH}› nm, Williamson-Hall**	**Strain × 10^{-4}(ε) %**		**Average Grain size (nm) ⟨D⟩**
0.05	206.496	-9.035		1047
0.10	212.909	-7.970		1138
0.15	258.705	-4.070		1246
0.20	283.878	-3.307		-
0.25	314.480	-2.455		-

Table 1 gives the lattice parameters a, c, the ratio c/a, and the cell volume of $MnBi_{1-x}Sb_x$ specimens as a function of antimony content. It can be seen that the lattice parameter declined linearly from ~8.692 to ~8.683 nm, as well as the lattice volume from ~656.756 to 654.537 nm^3 as x increasing from 0.05 to 0.25 at% for the Mn-Bi-Sb ternary phase. Regarding the binary phase (Mn_2Sb) and the single-phase (Bi), the same behavior of the lattice parameters (a and c) and the cell volume (v) declined with Sb content (as seen in Table 1). This means that the lattice shrinks and the Mn-Sb bond decreased with Sb content due to the ionic radius of Sb (76Å) is smaller than the ionic radius of Bi (103 Å)

The average crystallite sizes using ⟨D⟩ and the strain ε = Δd/d of the materials were calculated from the XRD results using the Williamson–Hall equation [19].

$$\beta cos\theta = \frac{K}{D} + 4\varepsilon\, sin\theta \quad (1)$$

Where β, K, λ, ε, θ are the full width at half maximum (FWHM), the grain shape factor (shape factor of 0.89), the X-ray wavelength, micro-strains (includes the effects of structural defects such as dislocations, stacking faults, twin boundaries and inter-grains), and the Bragg diffraction angle, respectively.

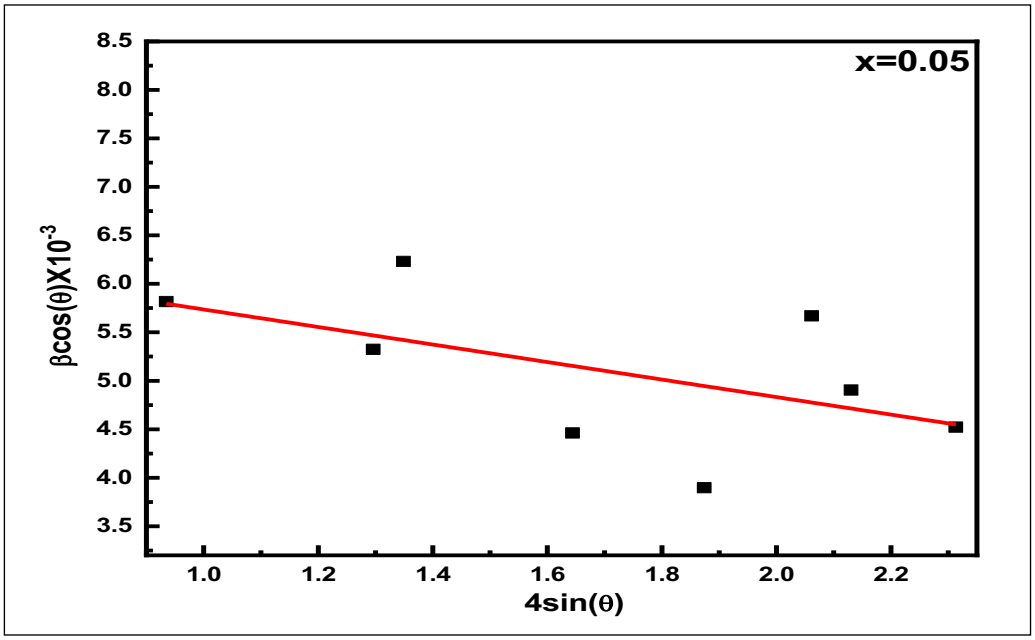

Fig. 2. Plots of βcosθ vs. 4sinθ for $MnBi_{0.95}Sb_{0.05}$ alloy, as an example.

The crystallite sizes are found to be in the range of 206.496 to 314.480 nm. The crystallite sizes increase with increasing Sb content (see Table 1 and Figure. 2). In addition, the strain ε increases with increasing Sb (-9.035E-4 to -2.455E-4 from x= 0.05 to 0.25) as in Table 1. This confirms previous results that the lattice shrinking due to Sb doping.

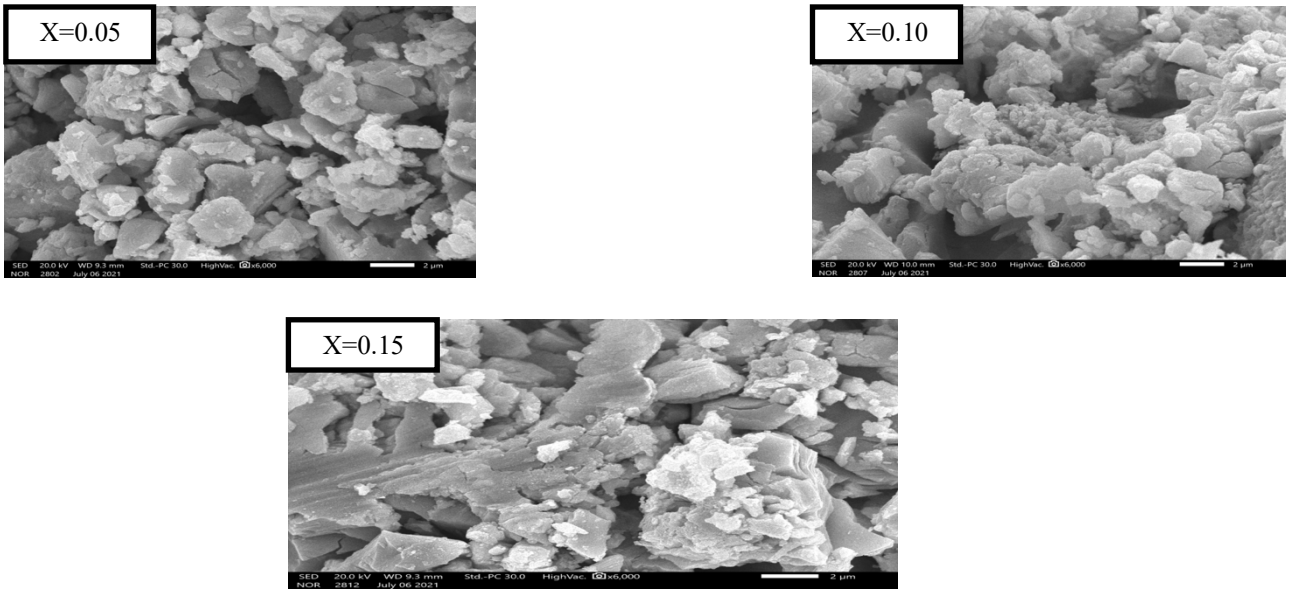

Fig. 3. SEM micrographs of $MnBi_{1-x}Sb_x$ (x= 0.05, 0.10 & 0.15 at. %)

Figure. 3 shows the scanning electron microscopy of three samples (x= 0.05, 0.10 & 0.15 at. %). It can be seen that there is a uniform distribution of grain sizes, and they are well-connected with each other. Slight porosity is observed at low Sb content, and the grain size of the samples increases with increasing Sb content, as in Table 1. In addition, it suggests that Mn-Bi-Sb with the gray section and Bi with the bright section.

Previous studies [20] have shown that the addition of the Sb element causes the appearance of MnSb / Mn_2Sb binary phases in the MnBiSb ternary matrix, and the granular fracture surfaces are well-developed. This means that the addition of the element Sb can separate the grain boundaries, which plays a role in suppressing the migration of grain boundaries during the solidification process, thus leading to grain refinement.

Clearly, the grain sizes observed by the SEM are several times larger than those calculated by the XRD, indicating that each grain determined by the SEM is composed of several crystallites.

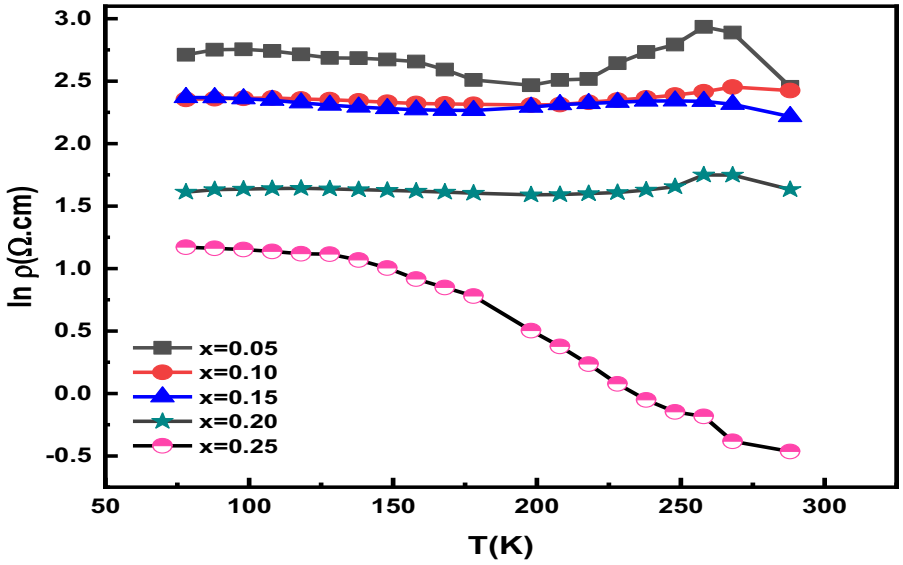

Fig. 4. Temperature dependence of resistivity for $MnBi_{1-x}Sb_x$ alloys

Figure 4 depicts typical electrical resistivity as a function of temperature for $MnBi_{1-x}Sb_x$ (x= 0.05, 0.10, 0.15, 0.20 &0.25) samples in the temperature range 80 -300 K. As shown in this figure, the decline of the resistivity value of the sample with increasing Sb content is due to the increased crystallite/grain sizes, which leads to the reduction of the grain boundaries. As in this figure, the electrical resistivity shows an extrinsic semiconductor behavior due to breaking covalent bonds, which leads to an increase in majority/minority carriers. With increasing temperature (near Curie temperature) the resistivity increases (metallic behavior) due to increased scattering and decreasing mobility of carriers. As in Figure 4, ρ(T) curve of x=0.25 behaves as an extrinsic semiconductor over the entire temperature range (as a high Sb content). This is because Sb can replace Bi that enters the unit cell and thus makes the alloy increase the semiconductor behavior and paramagnetic behavior.

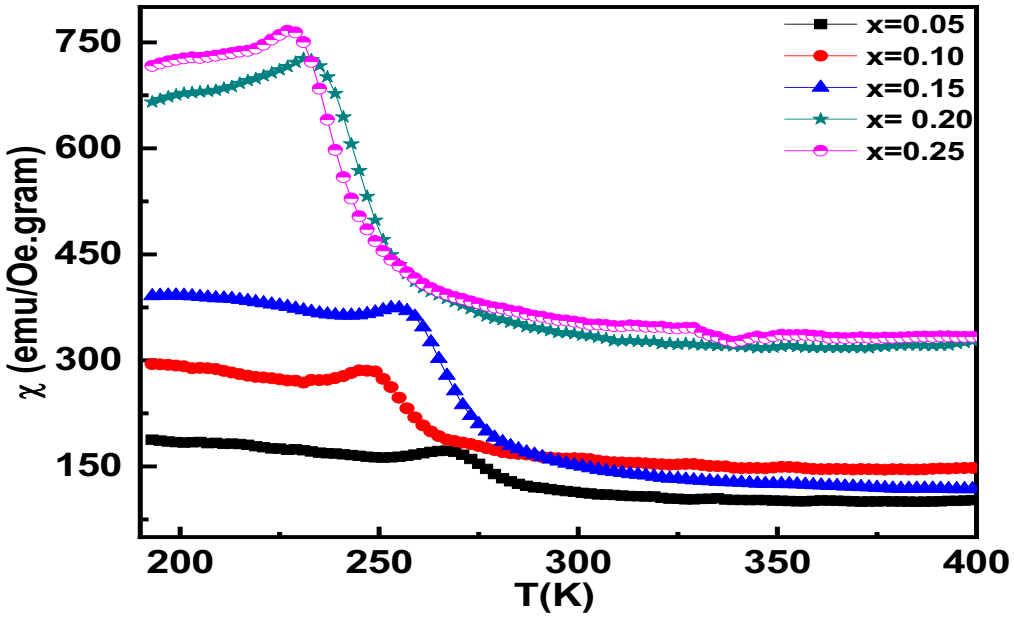

Fig. 5. Temperature dependence of susceptibility for $MnBi_{1-x}Sb_x$ alloys

AC magnetic susceptibility χ was measured on $MnBi_{1-x}Sb_x$ alloys from 100 K to 400 K is shown in Figure. 5. All samples verify Ferro- Paramagnetic transition at a certain temperature, Curie temperature (T_C). It can be seen that the

ferromagnetic behavior originates from the manganese atoms in the BiSb matrix because the Bi and Sb atoms have a small and opposite magnetic moment than the Mn atoms [21,22].

On the other side, the value χ increases with increasing Sb doping. For the five alloys, it is observed that the broad phase transition indicates an inhomogeneous magnetic state, which may be due to a high concentration of defects and their inhomogeneous distribution. The increase in antimony leads to a decrease in T_C, and thus a reduction in the extent of the ferromagnetic region, which is consistent with the change of metallic electrical conductivity to a semiconductor change. This is due to the increase in grain size, leading to a reduction in grain boundaries and magnetic order that weaken the ferromagnetic region.

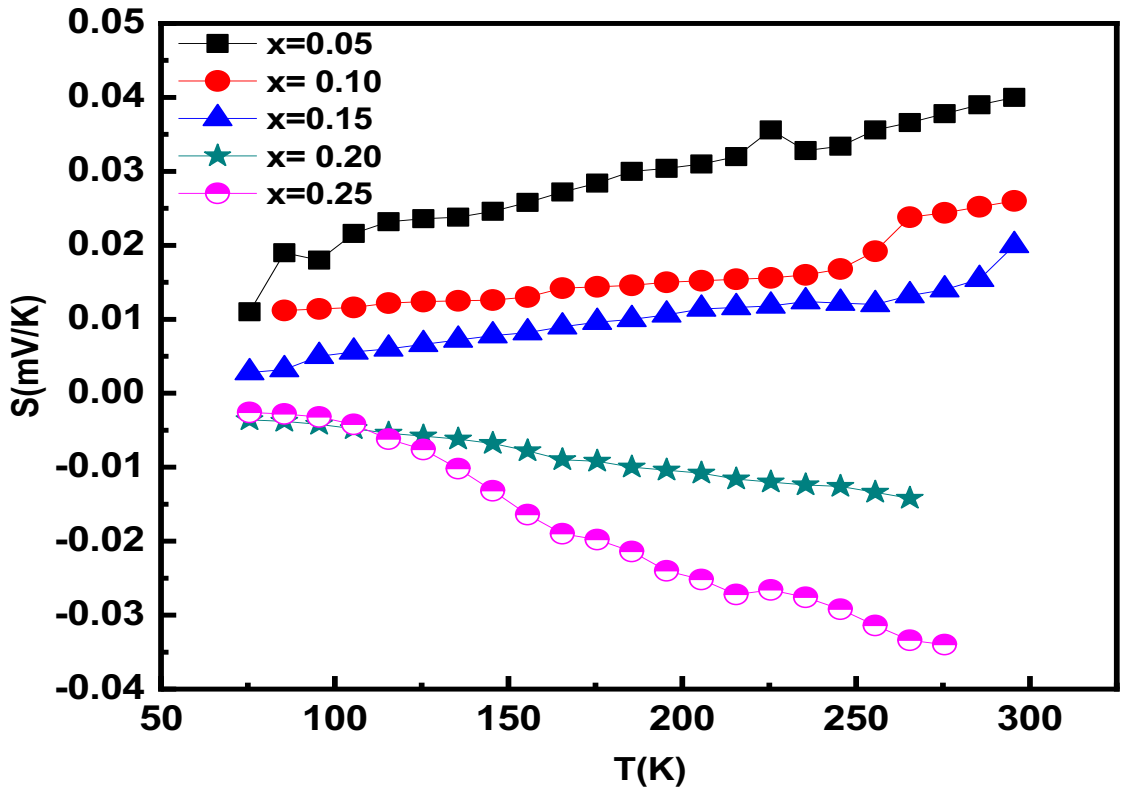

Fig. 6. S versus T for $MnBi_{1-x}Sb_x$ alloys

Figure. 6 shows the temperature dependence of the Seebeck coefficient for $MnBi_{1-x}Sb_x$ samples. The absolute Seebeck coefficient increases with increasing ambient temperature for all alloys. In addition, the Seebeck coefficient value has a positive and changes to a negative sign for x > 0.15. Replacing Bi with Sb increases the ability to accept more electrons, which leads to the excess of electrons than positive charges in the alloy. This is due to Sb has a higher electronegativity value (2.05) than Bi (2.02).

The thermal conductivity, k, of a metal or alloy usually is considered to be the sum of the electronic thermal conductivity, k_e , and thermal conductivity lattice, k_{lat}, components: $k = k_e + k_{lat}$.

Our alloys are degenerate semiconductors, which are closest to the metals. The contribution of $k_{lat} << k_e$ in the total thermal conductivity of our alloys [23], especially at high temperatures. This is mainly because of the increased scattering from the other phases and the increased presence of structural defects in the MnBi matrix [24-26]. According to Wiedemann–Franz law, we calculated the electronic thermal conductivity (k_{el})

$$k_{el} = L\sigma T \quad (2)$$

where L is Lorentz number 2.44×10^{-8} $W\Omega K^{-2}$ (degenerate limit), σ is the electrical conductivity, and T is the ambient temperature). As can be seen from Table (2) that the calculated values of k_e at RT for all alloys have an un-sequenced change with Sb content.

Table 2: Curie Temperature and electronic thermal conductivity of $MnBi_{1-x}Sb_x$ ($0.05 \leq x \leq 0.25$) alloys

Sample(x)	T_c-χ (K)	ρ_{RT} (Ω.cm)	$K_{electronic}$ ($W \cdot m^{-1} \cdot K^{-1} x10^{-5}$)
0.05	277	11.097	0.066
0.10	255	5.149	0.141
0.15	265	8.821	0.082
0.20	243	8.533	0.085
0.25	237	0.628	1.150

We estimated the figure of merit (ZT) of alloys (at high temperatures in our range) using the calculated k_e, where the k_e is the majority of thermal conductivity (as seen in Table 2). Notice that the lowest value of ZT is 1.45E-08 for the sample x = 0.10, while the highest value of ZT is 5.27E-02 for x = 0.25 at room temperature. Therefore, we consider our alloys to be possibly good thermoelectric materials for industrial applications.

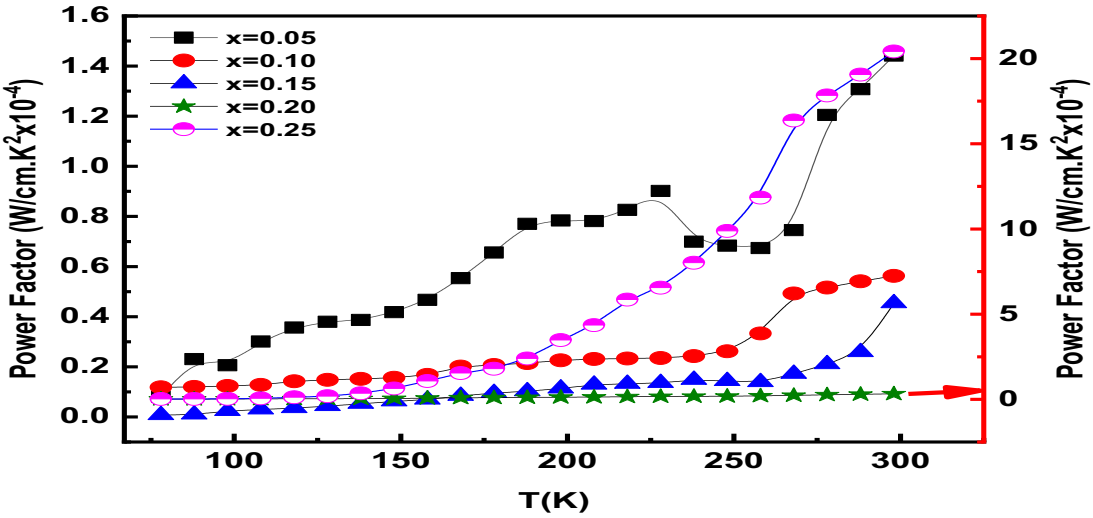

Fig. 7. Temperature dependence of Power factor of $MnBi_{1-x}Sb_x$ alloys

The thermoelectric power factor (PF) was calculated at all temperature ranges for five alloys ($MnBi_{1-x}Sb_x$) and plotted in Figure 7. The PF value increases with increasing temperature for all samples. On the other hand, the highest doping of Sb (x= 0.25) achieved the highest value of PF at RT (PF=0.204 μW/mK^2).

This finding leaves open the possibility of a further increase in ZT of the $MnBi_{1-x}Sb_x$ alloys through the use of increasing Sb doping, thus reducing the electronic thermal conductivity and increasing the Seebeck coefficient, which leads to an improvement in the figure of merit.

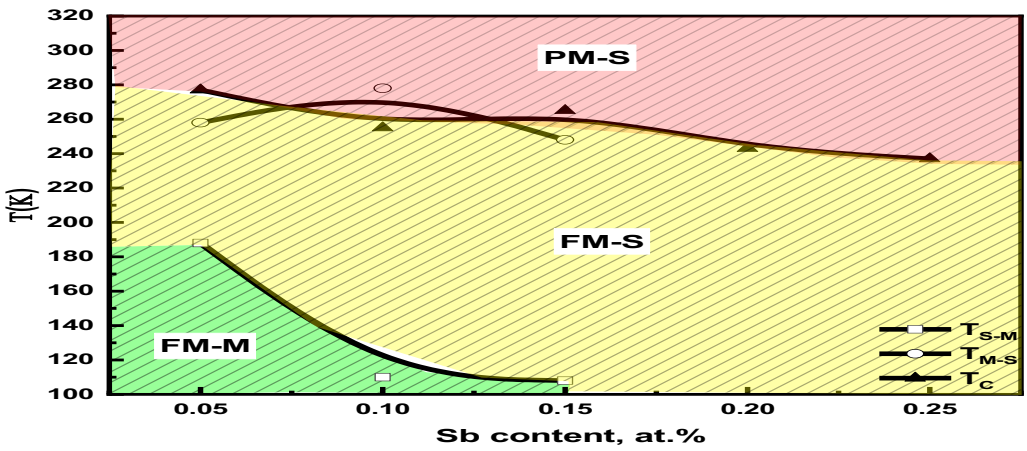

Fig. 8. Electrical-magnetic diagram of $MnBi_{1-x}Sb_x$ alloys

The transition temperature (metal to semiconductor, T_{M-S}/semiconductor to metal, T_{S-M}) and Curie temperature (T_C) were deduced from ρ(T) and derivatives of the magnetic susceptibility curves, respectively. The evolution of T_{M-S} and T_{S-M} and T_C is shown in Figure 8. This figure illustrates the electrical-magnetic diagram of the $MnBi_{1-x}Sb_x$ system, where the ferromagnetic metal (FM-M) phase underlies T_{S-M} (green line), the ferromagnetic semiconductor (FM-S) phase lies between T_{M-S} (yellow line) and T_C (red line), finally, the PM-S phase is above T_C (red line).

4. Conclusion

Polycrystalline $MnBi_{1-x}Sb_x$ was successfully synthesized using the conventional melt technique in the two-step synthesis process. The XRD results show that the crystal structure of the ternary phase with the composition $MnBi_{1-x}Sb_x$ as hexagonal P63/mmc group. Furthermore, the second phase Mn_2Sb is associated with the tetragonal P4/n mm and the bismuth phase similar hexagonal R-3m.

The electrical and magnetic properties have shown that Sb doping can replace Bi entering the unit cell and thus making the alloys tend to be semiconductors and decreases T_C. From TEP measurements, it was observed that the value of S decreased with Sb content and turns into a negative value for $x > 0.15$ at %. Finally, Sb dopant plays an important role in making these alloys applicable in the thermoelectric industry.

5. Acknowledgement

This work was funded by the Academy of Scientific Research and Technology, Egypt, under Science UP grant No. (6482). The authors acknowledge with thanks the Academy of Scientific Research and Technology for financial support.

Conflict of interest:

The authors declare that there is no conflict regarding the publication of this paper.

References

[1] M Kramer, R McCallum, I Anderson, S Constantinides. Prospects for non-rare earth permanent magnets for traction motors and generators. Jom, 64(7), 752-763. (2012).

[2] M Marker, P Terzieff, P Kainzbauer, M Bobnar, K Richter, H Ipser, BiMn: Synthesis, separation by centrifugation, and characterization. Journal of Alloys and Compounds, 741, 682-688. (2018).

[3] Y Liu, J Zhang, G Jia, X Zhang, Z Ren, X Li, C Jing, S Cao, K Deng, Magnetic anisotropy properties and spin reorientation for textured Bi− Mn alloys fabricated by a field-inducing technique. Physical Review B, 70(18), 184424. (2004).

[4] N Rama Rao, A Gabay, G Hadjipanayis, Anisotropic fully dense MnBi permanent magnet with high energy product and high coercivity at elevated temperatures. Journal of Physics D: Applied Physics, 46(6), 062001. (2013).

[5] J Cui, J Choi, G Li, E Polikarpov, J Darsell, N Overman, M Olszta, D Schreiber, M Bowden, T Droubay, M Kramer, N Zarkevich, L Wang, D Johnson, M Marinescu, I Takeuchi, Q Huang, H Wu, H Reeve, N Vuong, J Liu, Thermal stability of MnBi magnetic materials. Journal of Physics: Condensed Matter, 26(6), 064212. (2014).

[6] Cui, J Choi, E Polikarpov, M Bowden, W Xie, G Li, Z Nie, N Zarkevich, M Kramer, D Johnson, D. Effect of composition and heat treatment on MnBi magnetic materials. Acta Materialia, 79, 374-381. (2014).

[7] Y Chen, G Gregori, A Leineweber, F Qu, C Chen, T Tietze, H Kronmüller, G Schütz, E Goering, Unique high-temperature performance of highly condensed MnBi permanent magnets. Scripta Materialia, 107, 131-135. (2015).

[8] M Ellner, Structural and Chemical Parameters of NiAs-Type Phases Containing Ni, Co and Fe. J. Less-Common Met., 48(1), 21-52. (1976).

[9] V Taufour, S Thimmaiah, S March, S Saunders, K Sun, T Lamichhane, M Kramer, S Bud'ko, P Canfield, Structural and ferromagnetic properties of an orthorhombic phase of MnBi stabilized with Rh additions. Physical Review Applied, 4(1), 014021. (2015).

[10] P Kainzbauer, K Richter, H Effenberger, G Giester, H Ipser, The ternary Bi-Mn-Sb phase diagram and the crystal structure of the ternary τ phase Bi0. 8MnSb0. 2. Journal of Phase Equilibria and Diffusion, 40(4), 462-481. (2019).

[11] N. P.Grazhdankina, I.V. Medvedeva, A. V. Pasheev & Y. S. Bersenev, Magnetic properties of alloys MnSb and Mn1. 11Sb after subjection to high pressures and temperatures. Soviet Journal of Experimental and Theoretical Physics, 54(3), 564. (1981).

[12] N. P.Grazhdankina & V. Pasheev, Magnetic properties of alloys MnSb and Mn, Sb after subjection to high pressures and temperatures. Zh. Eksp. Teor. Fiz, 81, 1064-1070. (1981).

[13] T. X.Nguyen, H.Van Pham & V. Van Nguyen, Effect of Sb substitution on structural and magnetic properties of MnBi based alloys. Physica B: Condensed Matter, 552, 190-194. (2019).

[14] Y.Yamaguchi, H.Watanabe & T.Suzuki, Polarized neutron diffraction study on the electronic state of MnSb. Journal of the Physical Society of Japan, 45(3), 846-854. (1978).

[15] H. F.Mohamed, A. M.Ahmed, , A. K. Diab & E. Y. Omar, Impact of aluminum on the Seebeck coefficient and magnetic properties of La0.7Ba0.3MnO3 manganites. Chemical Physics Letters, 726, 22-28. (2019).

[16] A. M.Gabay, G. C Hadjipanayis & J. Cui, Effect of Sb substitution on crystal structure, texture and hard magnetic properties of melt-spun MnBi alloys. Journal of Alloys and Compounds, 792, 77-86. (2019).

[17] W. B. Pearson, The Cu2Sb and related structures. Zeitschrift für Kristallographie-Crystalline Materials, 171(1-4), 23-40. (1985).

[18] P.Cucka & C. S. Barrett, The crystal structure of Bi and of solid solutions of Pb, Sn, Sb and Te in Bi. Acta Crystallographica, 15(9), 865-872. (1962).

[19] G. K.Williamson & W. H. Hall, X-ray line broadening from filed aluminium and wolfram. Acta metallurgica, 1(1), 22-31. (1953).

[20] C. Bae, G.Lee, M. K.Kang, H.Lee, K.W. Moon, , & J.Kim, Synthesis and magnetic properties of Sb added MnBi magnets for applications at sub-zero temperatures. Journal of Alloys and Compounds, 899, 163365 (2022).

[21] J. B.Yang, , Y.B.Yang, X.G. Chen, X.B. Ma, J. Z. Han, Y. C.Yang & D. F. Chen, Anisotropic nanocrystalline MnBi with high coercivity at high temperature. Applied Physics Letters, 99(8), 082505. (2011).

[22] L .Zhiqiang, L.Helie, L.Wuyan, Z. Zhi & Z. Qingqi, Electronic structure and magnetic properties of MnBi (Al, Nd). Solid state communications, 79(10), 791-794. (1991).

[23] M. C. Nicolaou, Thermoelectric figure of merit of degenerate and nondegenerate semiconductors (Doctoral dissertation, Northeastern University). (2009).

[24] Y.Ma, Q.Hao, B.Poudel, Y.Lan, B.Yu, D.Wang & Z. Ren, Enhanced thermoelectric figure-of-merit in p-type nanostructured bismuth antimony tellurium alloys made from elemental chunks. Nano letters, 8(8), 2580-2584. (2008).

[25] L. P. Hu, T. J.Zhu, Y. G Wang, H. H. Xie, Z. J.Xu & X. B. Zhao, Shifting up the optimum figure of merit of p-type bismuth telluride-based thermoelectric materials for power generation by suppressing intrinsic conduction. NPG Asia Materials, 6(2), e88-e88. (2014).

[26] B. Cao, J. Jian, B.Ge, S. Li, H.Wang, J. Liu, , & H. Zhao, Improved thermoelectric performance in p-type Bi0.48Sb1.52Te3 bulk material by adding MnSb2Se4. Chinese Physics B, 26(1), 017202. (2017).